Title

Effect of surface termination on the balance between friction and failure of Ti3C2Tx MXenes

Journal

npj Materials Degradation, 7(1)

ISSN

2397-2106

Authors

Yang, Quanpeng
Eder, Stefan J
Martini, Ashlie
et al.

Publication Date

2023

DOI

10.1038/s41529-023-00326-9

Peer reviewed

ARTICLE OPEN

Check for updates

Effect of surface termination on the balance between friction and failure of $Ti_3C_2T_x$ MXenes

Quanpeng Yang[1], Stefan J. Eder[2,3]✉, Ashlie Martini[1] and Philipp G. Grützmacher[2]

Reactive molecular dynamics simulations of $Ti_3C_2T_x$ with three different surface terminations were used to understand friction and failure of MXenes during sliding at normal pressures from 2–20 GPa and temperatures from 300–1100 K. The O-terminated MXene had the smallest shear stress at low pressures and temperatures, but failed at more severe conditions due to interlayer bonding and the formation of Ti–O–Ti bridges between MXene layers. Failure was not observed for the OH-terminated MXene or a heterostructure combining O- and OH-terminations. For these, at less severe operating conditions, shear stress was smaller for the OH-terminated MXene, while the opposite was observed at higher temperatures and pressures. These trends were explained in terms of adhesion and the complex effect of hydrogen atoms that can either facilitate or hinder sliding, depending on the termination and conditions. Results show that friction and failure are affected by and potentially tunable via MXene surface termination.

npj Materials Degradation (2023)7:6 ; https://doi.org/10.1038/s41529-023-00326-9

INTRODUCTION

The dimensional characteristics of a material dramatically affect its properties[1]. Two-dimensional (2D) materials are a class of materials characterized by atomically thin layers with strong chemical bonds in-plane, but only weak out-of-plane coupling between individual layers[2]. The successful isolation of graphene by mechanical exfoliation has spurred research in the field of 2D materials, and entirely new members of this material class are being discovered each year[3]. 2D materials possess high specific surface areas such that charge and heat transport are confined to a plane[1], and they have been shown to exhibit extraordinary electrical, mechanical, and chemical properties[4]. As such, this class of materials is fascinating for its potential use in a broad range of applications, including energy storage, photonics, superconductors, flexible electronics, sensors, and tribology[5,6].

One important application of 2D materials is as solid lubricants. In this role, the weak interactions between layers of 2D materials result in low shear strength and correspondingly low friction and wear[7]. A prominent example of this class of materials is molybdenum disulfide (MoS_2), which has long been used as a solid lubricant and is frequently utilized for space applications[8]. Another well-known 2D solid lubricant is graphene, which is already in common use as a coating, liquid lubricant additive, or as one component of self-lubricating nano-composite materials[9]. Given the right conditions, even superlubricity (i.e., a coefficient of friction <0.01) can be achieved with 2D materials[10]. However, a drawback of solid lubricants is their sensitivity to the environment. In particular, MoS_2 and graphite are quite sensitive to humidity[9]. The applicability of MoS_2 is limited if oxygen or water molecules are present, whereas graphite only functions well if the surrounding air is humid. Moreover, most conventional solid lubricants are easily worn out, exhibiting poor wear life[11].

Another class of 2D materials that has only recently begun to be considered for tribological applications is MXenes[12–14]. MXenes are layered transition metal carbides, nitrides, and carbonitrides. They are described by the chemical formula $M_{n+1}X_nT_x$ ($n = 1$–4), where M represents the transition metal atom (groups 3–6 of the periodic table), X can be carbon or nitrogen, and T_x indicates the surface termination[15]. MXenes have been increasingly used in solid lubrication, liquid lubrication, and as reinforcement phase in composites[16]. Recently, Grützmacher et al. demonstrated that MXenes can outperform the more common 2D nanomaterials in terms of wear life[17].

A variety of different MXenes can now be synthesized[15]. Although many properties of MXene materials, such as chemical composition, atomic layer number, and flake size, can be tuned, it is difficult to produce stable MXenes with homogeneous surface termination[18]. With conventional synthesis strategies, MXenes typically exhibit a random mix of different terminations, which will directly affect their behavior in a sliding application. However, using molten salt etching, uniformly terminated MXenes (-Cl, -Br, -I) can be obtained. Since these terminations are less strongly bonded to the M atoms than the typical terminations (-F, -OH, -O), they can subsequently be replaced to produce other types of termination or even bare MXenes[18]. Given the expected significant effect of surface termination on interlayer sliding of MXenes, it is desirable to understand how the various terminations affect tribological behavior[19,20].

The dimensional characteristics of 2D materials lend themselves extremely well to analysis using molecular dynamics (MD) simulation. Early MD modeling of MXenes focused on their mechanical properties[21], thermal stability[22], or energy storage potential[23]. Only recently has MD been applied to study the frictional properties of this promising material class, focusing either on operation at cryogenic and room temperature[24] or on a single termination[25]. In this work, we used reactive MD simulations, i.e., simulations based on an empirical potential that captures the formation and breaking of chemical bonds, to characterize and understand the effects of surface termination on friction and wear of MXenes over a wide range of temperatures and pressures. This constitutes a significant contribution to the field, particularly since solid lubricants are usually used under

[1]Department of Mechanical Engineering, University of California-Merced, 5200 N. Lake Road, Merced 95343 CA, USA. [2]Institute for Engineering Design and Product Development, TU Wien, Lehárgasse 6 - Objekt 7, 1060 Vienna, Austria. [3]AC2T research GmbH, Viktor-Kaplan-Straße 2/C, 2700 Wiener, Neustadt, Austria. ✉email: stefan.j.eder@tuwien.ac.at

harsh conditions, markedly exceeding the conditions in previous modeling studies. We constructed computational models of self-mated $Ti_3C_2T_x$ MXene layers with two different types of terminations, as well as a heterostructure consisting of a mixture of the two terminations. Over 600 different simulation cases were run and analyzed. The effect of termination on pressure- and temperature-dependent shear stress and, in some cases, failure, was explained in the context of interlayer interactions and bonding.

RESULTS AND DISCUSSION

Shear stress results

Frictional resistance to sliding was characterized as shear stress for three bilayer $Ti_3C_2T_x$ MXene models: both layers terminated with O, both layers terminated with OH, or one layer terminated with O and the other with OH (called heterostructure in this work). The average shear stress as a function of their surface termination (OH, O, heterostructure), pressure (2–20 GPa), and temperature (300–1100 K) is presented in Fig. 1; the data is also presented as contour plots in Supplementary Fig. 1. Close-up views of the interface before loading are shown in the inset of each figure. At 300 and 500 K and pressures below 8 GPa, shear stress is smallest for the O-terminated MXene. However, at all other conditions, the O-terminated MXene has the largest shear stress. This indicates that the presence of OH termination on either one or both MXene layers can reduce the shear stress compared to O-terminated, self-mated MXenes. The OH-terminated and heterostructure MXenes have similar shear stress, except at the lower temperatures where the shear stress is larger for the heterostructure.

Temperature affects shear stress in some of the simulation cases. There is little effect of temperature on the OH-terminated MXene, except at the highest pressures where the shear stress is largest at 300 K. For the heterostructure MXene, shear stress is larger at lower temperatures. Lastly, for the O-terminated MXene, shear stress increases with increasing temperature at low pressures, a trend opposite to that of the other two MXenes. At high pressures, there is no statistically significant temperature dependence for the O-terminated MXene.

In all cases, regardless of surface termination, the shear stress generally increases with pressure, resulting from an increase in shear strength of the interface as the two MXene layers are pressed together. For the OH-terminated MXene and the heterostructure, shear stress increases steadily with pressure. The same trend of shear stress increasing with pressure is observed for the O-terminated MXene at the two highest temperatures of 900 and 1100 K, although large shear stress is observed even at the lowest pressure of 2 GPa. In contrast, for the O-terminated system at temperatures below 900 K, there are sudden transitions to larger shear stress, and the pressure at which this transition occurs decreases with increasing temperature.

Origin of interlayer failure

The transition to a larger shear stress for the O-terminated MXene is associated with interlayer bonding and failure. This was characterized by the number of bonds formed between atoms in the opposing MXene layers. Except for a few Ti–C and C–O bonds, most of these bonds are Ti–Ti or Ti–O (Supplementary Fig. 2), pointing to the origin of the large shear stress in O-terminated MXenes as the formation of Ti–O–Ti bridges (illustrated in Supplementary Fig. 3). The number of Ti–O–Ti bridges in the O-terminated MXene at the end of each simulation is shown in Fig. 2a. For the lowest pressures and temperatures, no bridges form, while, at the two highest temperatures, bridges are formed at any pressure. For temperatures of 300, 500, and 700 K, there is a transition from no or little bonding to many interlayer bonds at

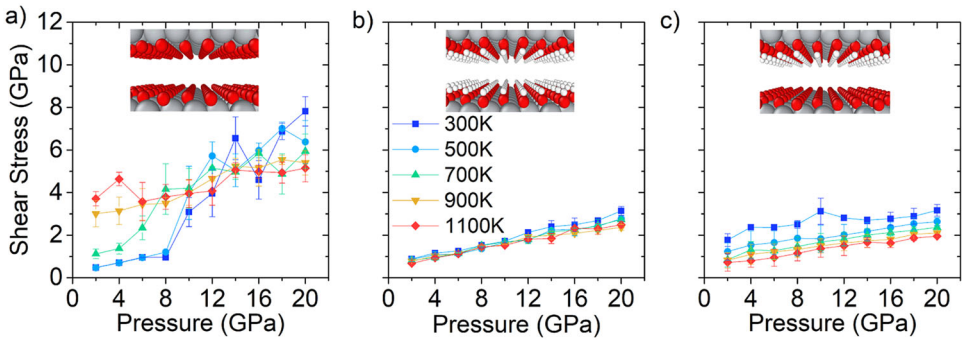

Fig. 1 MXene shear stresses. Shear stress of **a** O-terminated, **b** OH-terminated, and **c** heterostructure MXenes as a function of pressure at 300, 500, 700, 900, and 1100 K. The insets are close-up views of the model MXenes before they are thermalized and loaded. The error bars reflect the standard error of three sliding cycles.

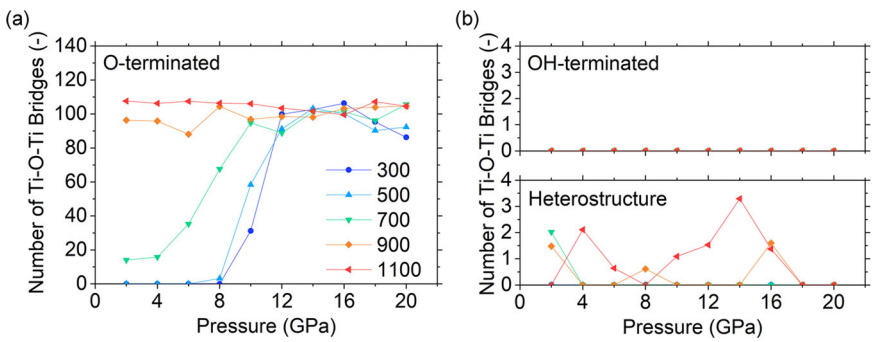

Fig. 2 Interlayer Ti–O–Ti bridges. Number of interlayer Ti–O–Ti bridges averaged over the duration of sliding for **a** O-terminated, **b** OH-terminated, and **c** heterostructure MXenes as a function of pressure at 300, 500, 700, 900, and 1100 K.

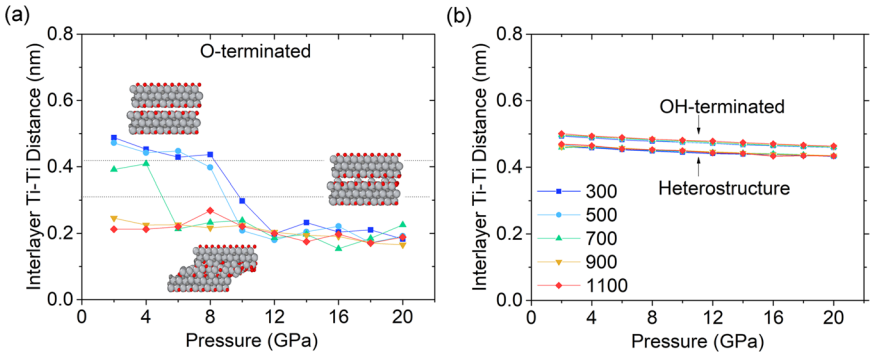

Fig. 3 Interlayer Ti–Ti distances. Interlayer Ti–Ti distance for **a** O-terminated MXenes, **b** OH-terminated and heterostructure MXenes as a function of pressure at 300, 500, 700, 900, and 1100 K. The insets in **a** are representative snapshots of the O-terminated model, from top to bottom, when there is no failure, as bonds start to form between the layers, and after failure.

10 GPa for 300 and 500 K, and at 6 GPa for 700 K. This indicates that the diffusion of O into one of the layers and subsequent formation of interlayers Ti–O bonds is facilitated by higher pressures and temperatures. Higher pressures correspond to smaller atomic distances, increasing the likelihood of diffusion as well as bond formation. Interlayer bond formation facilitated by high pressure has been reported for other 2D materials, such as graphene[26], hBN[27], and TMDs[28]. Similarly, temperature enhances diffusion and the rate of bond formation due to the availability of more thermal energy.

To corroborate these results, the interlayer distance between O-terminated MXene layers was calculated as the position of the first peak of the distribution of *z*-direction distances between Ti atoms of opposing MXene layers. The interlayer distance in Fig. 3a decreases from around ~0.4 to ~0.2 nm at the same pressures and temperatures at which more Ti–O–Ti bridges start to form. Both the number of Ti–O–Ti bridges and the interlayer distance trends correlate well with the transition to larger shear stress in Fig. 1a. Below the transition pressure and temperature, the MXene layers remain separated and slide easily relative to one another, hence providing smaller shear stress. When the interlayer distance is reduced and chemical bonds form, however, their easy-to-shear ability is lost, leading to large shear stress.

Interestingly, if only a few bridges form, such as seen in the transition regime at 8 GPa and 500 K (Fig. 2a), the interlayer distance does not decrease dramatically (Fig. 3a), and there is no jump in shear stress. As long as there is sufficient spacing between the layers, catastrophic failure associated with extremely large shear stress does not occur, at least not within the short sliding time of 400 ps considered here. Nevertheless, these isolated bonds mark the beginning of failure of the MXene system, and a slight increase in temperature or pressure results in failure. Therefore, the formation of chemical bonds between layers is indicative of failure of the material as a solid lubricant and is likely to correspond to the onset of mechanical degradation of the MXenes, as described, for instance, in ref. [17], which ultimately might lead to reduced wear life of MXene solid lubricant coatings.

The same interlayer bond analysis was performed for the OH-terminated and heterostructure MXenes, as shown in Fig. 2b. No Ti–O–Ti bridges form at any pressure or temperature for the OH-terminated MXene. For the heterostructure, only a few bridges form at the highest temperatures. This is again consistent with the interlayer distances for the OH-terminated and heterostructure MXenes in Fig. 3b, which decrease gradually with increasing pressure, but are between 0.4 and 0.5 nm at any temperature or pressure, confirming effective separation of the MXene layers. The interlayer distance is slightly larger for the OH-terminated case, because the OH groups require more space than the O in the heterostructure. This is in accordance with previously reported interlayer distances, which were smaller for OH-terminated MXenes than for O-terminated MXenes[29]. However, we do not observe any clear correlation between interlayer distance and shear stress, as previously reported for MXenes[30] or graphene[31]. For both the OH-terminated and heterostructure MXenes, there is little interlayer bonding (Supplementary Fig. 2) such that these MXenes are able to maintain stable shear stress even at high temperatures and pressures. It is possible that the surface H atoms additionally stabilize the layer structure to such an extent that the formation of interlayer Ti–O–Ti bridges is impeded. As the heterostructure MXene contains fewer H atoms, this stabilization of the structure is less pronounced, and a few bonds form at very high temperatures, but these isolated bonds have little effect on the interlayer distance or shear stress.

Friction mechanisms during wearless sliding

A good tribological system should not be operated under conditions at which failure occurs, so we next analyzed the shear stress results only for cases where the interlayer distance was above 0.3 nm, i.e., all the OH-terminated and heterostructure MXenes, and the O-terminated MXene at low temperatures and pressures (Fig. 3). A comparison of the shear stress for the three MXenes under conditions where no failure was observed is shown in Fig. 4. At low pressures and temperatures, where the O-terminated MXene did not fail, it has the smallest shear stress. Comparing the OH-terminated and heterostructure MXenes at 300 K and pressures up to 12 GPa, the OH-terminated MXene has smaller shear stress. At higher pressures and 300 K, as well as at any pressure for temperatures between 500 and 900 K, there is no statistically significant difference between these two systems. At the highest temperature of 1100 K and pressures above 14 GPa, the heterostructure shear stress is smaller than that of the OH-terminated MXene. Also, at the three higher temperatures, the slope of the shear stress vs. pressure curve (similar to the macroscopic concept of friction coefficient) is smaller for the heterostructure than for the OH-terminated MXene (Supplementary Table 1). These trends were analyzed in terms of the interlayer binding energy and dehydrogenation of the surface termination.

For wearless sliding, frictional resistance is dominated by adhesion. Adhesion in 2D materials can be directly related to the binding energy between adjacent layers. It has been shown that binding energy and, therefore, interlayer force, is weakened by providing MXenes with surface terminations (compared to bare MXenes such as Ti_3C_2), and that the interactions between the layers are largely governed by the surface terminations[19,20]. The binding energies of the three MXenes considered here were calculated previously using first-principles calculations and the weakest interactions were found for the O-terminated MXene[19,20]. To evaluate this in our simulations, we calculated adhesion from

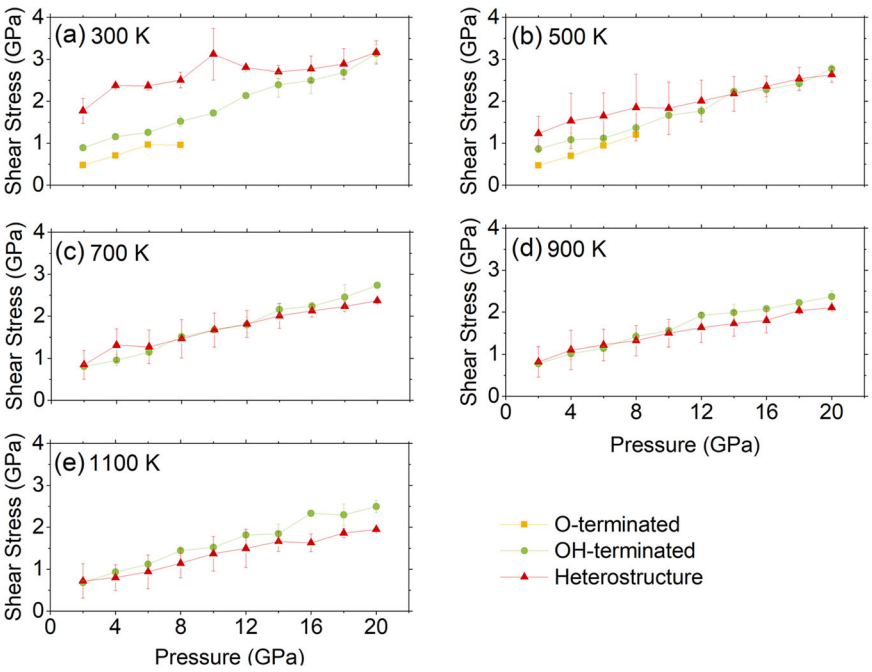

Fig. 4 Shear stresses at conditions without MXene failure. Shear stress between O-terminated, OH-terminated, and heterostructure MXenes as a function of pressure at **a** 300, **b** 500, **c** 700, **d** 900, and **e** 1100 K for conditions at which no failure occurred. The error bars reflect the standard error of three sliding cycles.

Table 1. Adhesive stress (in GPa) calculated from the intercept of linear fits to the data in Fig. 4.

MXene	300 K	500 K	700 K	900 K	1100 K
O-terminated	0.35	0.22	–	–	–
OH-terminated	0.60	0.59	0.57	0.67	0.53
Heterostructure	2.03	1.17	0.84	0.78	0.57

the intercept of linear fits of the shear stress vs. pressure data, i.e., the shear stress offset at zero pressure[32]. The resulting adhesive stresses are given in Table 1.

Generally, adhesion decreases with temperature, which might be a result of increased vibrational energy of the atoms, leading to weakening of van der Waals interactions[33]. This decrease in adhesion is also reflected by the smaller shear stress at higher temperatures for the OH-terminated and heterostructure MXenes in Fig. 1. The adhesive stress is lowest for the O-terminated MXene and highest for the heterostructure at any temperature. The low binding energy and adhesion for O-terminated MXenes has been associated with localization of electrons around the O atom, leading to electrostatic repulsion between the O-terminated MXene layers[34]. This is consistent with our results that show, for cases where there is no failure, the shear stress for the O-terminated MXenes is the smallest among the three MXenes (Fig. 4a, b). Comparing the heterostructure and OH-terminated MXenes, the adhesion is higher for the heterostructure and the difference is larger at lower temperatures. The adhesion trend is consistent with the higher shear stress of the heterostructure at 300 K and lower pressures (Fig. 4a).

The adhesion trends in Table 1 may be explained by van der Waals forces and the formation of interlayer hydrogen or dihydrogen bonds. The O-terminated MXenes are dominated by van der Waals forces since no (di)hydrogen bonds are possible due to the lack of available H atoms in our ideal model systems. OH-terminated MXenes have been shown to form weak dihydrogen bonds in a previous study[20], and the heterostructure modeled

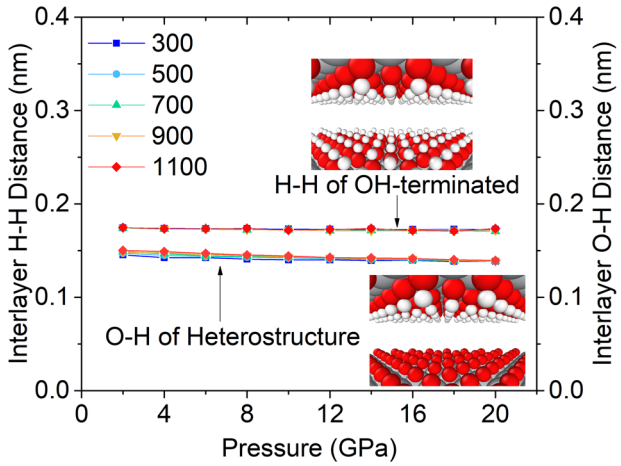

Fig. 5 Interlayer H–H and O–H distances. Interlayer termination–termination distance for the OH-terminated (H–H distance) and heterostructure (O–H distance) MXenes as a function of pressure at 300, 500, 700, 900, and 1100 K averaged over the duration of sliding. The insets are zoomed-in views of the corresponding MXene models prior to thermalizing and loading.

here may form hydrogen bonds. This was evaluated in the simulations from the interlayer O–H distance for the heterostructure and the H–H distance for the OH-terminated MXene, as shown in Fig. 5. For the OH-terminated MXene, the interlayer H–H distance of ~0.17 nm agrees well with the published data of 0.173 nm (simple hexagonal stacking)[20], indicating the presence of dihydrogen bonds. For the heterostructure, the interlayer O–H distance is below 0.15 nm, which falls within the range of strong hydrogen bonds (0.12–0.15 nm)[35], and therefore indicates formation of hydrogen bonds for this MXene. The hydrogen bonds in the heterostructure are stronger than the dihydrogen bonds in the OH-terminated MXene, which may explain why the adhesion is larger for the heterostructure.

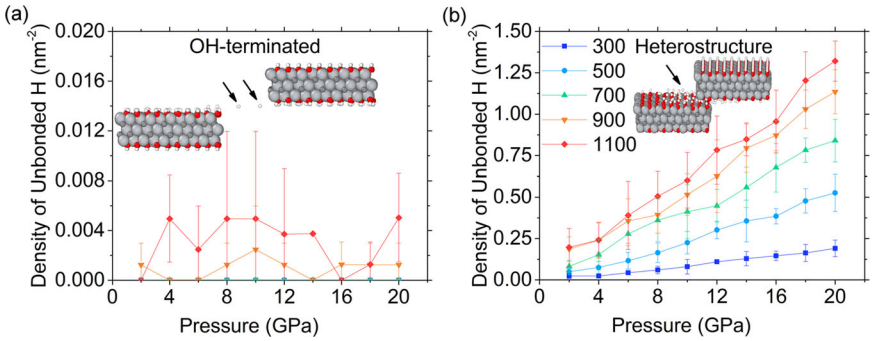

Fig. 6 Unbonded hydrogen atom densities. Density of unbonded H atoms for the **a** OH-terminated and **b** heterostructure MXenes as a function of pressure at 300, 500, 700, 900, and 1100 K averaged over the duration of sliding. The inset snapshots of both MXenes are from a simulation performed at 1100 K and 2 GPa. The error bars reflect the standard error of three sliding cycles.

Adhesion explains the small shear stress of the O-terminated and OH-terminated MXenes at low temperatures, but the trend is not consistent with the smaller shear stress of the heterostructure at high temperatures. This suggests there is another factor contributing to the sliding resistance of these MXenes. Dehydrogenation has been seen previously in simulations of sliding at Si–Si or DLC–diamond interfaces[36,37]. To quantify the potential effect of dehydrogenation here, the percentage of broken O–H bonds and the density of unbonded hydrogen atoms was calculated by averaging the number of hydrogen atoms with no covalent bond over time and then dividing by the nominal contact area. As shown in Supplementary Fig. 4, for both OH-terminated and heterostructure MXenes, higher pressures and, in particular, higher temperatures lead to more hydrogen atoms being sheared from the surface. However, for the heterostructure, this process starts at a lower temperature, and the density of unbonded hydrogen atoms is much higher at any pressure or temperature condition. In the case of the OH-terminated MXene, both layers are saturated with hydrogen atoms, resulting in a lower tendency to break O–H bonds. On the other hand, during sliding of the heterostructure MXene, the formation of strong hydrogen bonds with the O-terminated layer lowers the activation energy required for breaking of O–H bonds on the OH-terminated layer. The removed hydrogen atoms can then either form covalent bonds with any free O atom of both MXene layers or remain unbonded between the layers, as shown in Fig. 6.

For the heterostructure at lower temperatures, few H atoms are removed from the upper layer, so there are strong interactions (i.e., hydrogen bonds) between O-terminated and OH-terminated layers, leading to the large shear stress. However, at higher temperatures, there are many H atoms that leave the upper layer and bond to the opposing layer such that both layers are (partially) terminated by OH groups (Supplementary Fig. 5). In these cases, the interface qualitatively resembles that of the OH-terminated MXene, which leads to weaker interactions and explains the similarity in the shear stress of both hydrogenated MXenes at high temperatures (Fig. 4). According to a recent experimental study, friction can be decreased by as much as 57% by reducing hydroxyl groups by 7% in favor of oxygen and fluorine[19]. For the heterostructure at high temperatures, the density of unbonded H atoms is high (Fig. 6), so the system contains fewer hydroxyl groups than if one of the surfaces were fully OH-terminated (i.e., the initial configuration of the heterostructure) at any given time. This implies that, in our simulations, there are fewer hydroxyl groups on the heterostructure at high temperatures, which leads to smaller shear stress than in the OH-terminated MXene.

As no atoms ever leave the system in our simulations, some of the H atoms removed from the heterostructure will immediately form stable bonds with the opposing layer, as described above. However, some remain for short periods of time as unbonded atoms trapped between the layers, possibly acting as a sort of lubricant[38]. Analyses indicate that H atoms are only unbonded for a few picoseconds, but there are continually new H atoms sheared from the surface, such that the system is in dynamic equilibrium with unbonded H atoms between the layers (Supplementary Fig. 6). Therefore, the observation that the density of unbonded H atoms increases with temperature and pressure for the heterostructure (Fig. 6) may explain why the slope of the shear stress vs pressure data is smaller for the heterostructure than the OH-terminated MXene (Supplementary Table 1). The H atoms that either rebond or remain temporarily unbonded seem to sufficiently stabilize the system such that, even though isolated Ti–O–Ti bridges form at the highest temperatures (Fig. 2), there is no failure and the shear stress is low (Fig. 4). This shows that the lubricating effect of the unbonded H atoms and the reduction of interlayer forces due to fewer hydroxyl groups for the heterostructure have a greater influence on the shear stresses than the formation of isolated interlayer bonds as long as the layers remain fully separated (Fig. 3).

Conclusions

In conclusion, our simulations showed that O-terminated, OH-terminated, and heterostructure MXenes exhibited distinct condition-dependent shear stress behavior. O-terminated MXenes had the smallest shear stress at low pressures and low temperatures, but showed a steep increase in shear stress above 6–8 GPa and 700–900 K due to interlayer bonding and subsequent failure. The latter could be correlated with the formation of Ti–O–Ti bridges between the MXene layers during sliding and a simultaneous drop in the interlayer distance by around 50%. The OH-terminated and heterostructure MXenes systems with hydrogen as part of their terminations did not fail at any of the studied pressure and temperature conditions, but their shear stress trends differed. While the shear stress in OH-terminated MXenes had almost no temperature dependence, heterostructures showed a clear decrease of shear stress with temperature, which was dominated by a decrease in the (pressure-independent) adhesive contribution to sliding resistance. The high adhesion in the heterostructure MXenes at low temperatures may be explained by the presence of hydrogen bonds, which are stronger than the dihydrogen bonds in the OH-terminated systems. With increasing pressure and temperature, the friction performance of the heterostructure becomes comparable to that of the OH-terminated MXene, finally surpassing it and exhibiting the lowest shear stress at the highest pressure and temperature. This could be explained by the hydrogenation of the O-terminated MXene layer as well as unbonded H atoms, both of which weaken interlayer interactions and therefore shear stress. Additionally, the free hydrogen atoms, whose number increased linearly with the temperature, possibly act as a lubricant. For future studies, it may

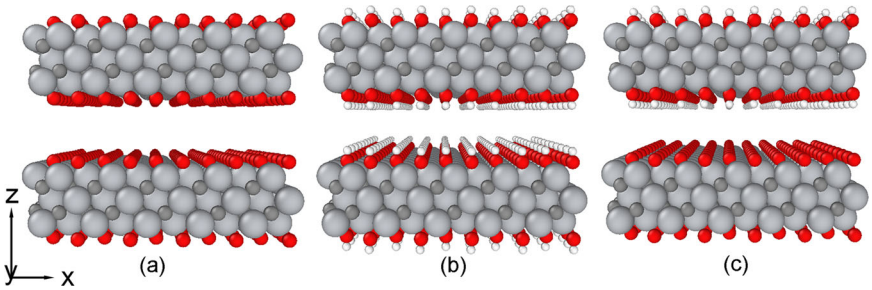

Fig. 7 MXene model overview. Atomistic models of **a** $Ti_3C_2O_2$, **b** $Ti_3C_2OH_2$, and **c** heterostructure MXenes. Atom colors correspond to: oxygen, red; carbon, dark gray; titanium, light gray; and hydrogen, white.

be interesting to add a variation of humidity to the parametric study, as this is one of the parameters that greatly affect the friction of MXenes and 2D materials in general. Macroscale experimental studies have demonstrated that high humidity (i.e., 80% rH) is detrimental to the tribological performance of MXenes[39], while in terms of failure, the intercalation of water molecules between hydrophilic MXene layers might prevent bond formation. It has been shown that MXenes even expand along the crystallographic c direction when compressed in the presence of water[40]. Generally, our results show that there is a termination-dependent balance between low shear stress and wear resistance. The findings provide a fundamental understanding of the effect of MXene surface termination on sliding behavior and may serve as a basis for selecting, or even designing, MXenes for a given application and expected operating conditions.

METHODS

Models of two layers of MXenes were built using Materials Studio[41] based on the Ti_3C_2 structure obtained from Materials Project[42]. Terminal groups were then added to create three model systems: both layers terminated with O, both layers terminated with OH, or one layer terminated with O and the other with OH (called heterostructure in this work). The atomistic models of these three MXenes are shown in Fig. 7. Periodic boundary conditions were applied in the *x*- and *y*-directions to mimic an ideal MXene with infinite surface area and without defects. The dimensions of the models in the *x*- and *y*-directions were 2.66 and 3.07 nm, respectively. The positions of the bottommost atoms in the lower MXene layer were fixed and the topmost atoms in the upper MXene were treated as a rigid body. Although the models in this study are approximations of synthesized MXenes with finite size and defects, the simulation methods developed here can be extended to more realistic model structures.

Reactive potentials enable MD simulations to capture the formation and breaking of chemical bonds at sliding interfaces[43]. Here, we tested the ReaxFF potential with four different parameterizations[23,44–46], but found that only one of them maintained stable structures for all three MXene terminations, see Supplementary Table 2. The chosen potential, developed by Osti et al.[23], has been successfully applied in MD simulations of titanium-containing materials, including titanium dioxide[44,47,48] as well as MXenes[23,49].

The MD simulations were carried out using LAMMPS (Large-scale Atomic/Molecular Massively Parallel Simulator)[50] and visualized using OVITO (Open Visualization Tool)[51]. The simulations were run in the NVT (constant number of atoms, volume, and temperature) ensemble, with the temperature controlled using a Nosé–Hoover thermostat[52], and with a time step of 0.25 fs. Each simulation consisted of two steps: loading and sliding (Supplementary Fig. 7). For loading, a normal force was applied to the top layer of the upper MXene, and the system was allowed to stabilize at the specified load for 25 ps. It was ascertained by monitoring the potential energy if the system had indeed reached a stable equilibrium state (Supplementary Fig. 8). The pressure was calculated from the load applied to the upper MXene divided by the nominal contact area, i.e., the *x*–*y* cross-section of the system. The rigid body at the top of the upper MXene was coupled with a virtual atom (an atom that does not interact with the other atoms via an interaction potential) using a harmonic spring with an elastic constant of 70 N m^{-1}. After loading, the virtual atom was moved along the *x*-direction at a constant speed of 20 m s^{-1} for 400 ps. The upper MXene was thus dragged by the virtual atom, making it slide against the lower MXene. During sliding, the center of mass of the upper MXene crossed the periodic boundary in *x* and continued sliding. The simulation was run until this sliding loop occurred three times. The simulations were performed at all possible combinations of ten pressures (2, 4, 6, 8, 10, 12, 14, 16, 18, and 20 GPa) and five temperatures (300, 500, 700, 900, and 1100 K), a total of 600 simulations amounting to approximately 1 million CPU-hours. The pressure range was selected to comfortably cover all the pressures that might be expected at the single-asperity level, while the temperatures were chosen to identify the applicability limits of MXenes by starting at room temperature and extending well beyond those temperatures where MXenes have been experimentally shown to decompose[53].

Shear stress was calculated as the lateral force divided by the nominal contact area between the two layers of MXenes (*x*–*y* cross-section of the system) and averaged over three sliding loops. Covalent bonds were identified and counted using the bond table generated during the ReaxFF simulation with a minimum bond order threshold of 0.3.

DATA AVAILABILITY

The data that support the findings of this study are available from the corresponding author upon reasonable request.

CODE AVAILABILITY

Code used to produce the findings in this study are available from the corresponding author upon reasonable request.

Received: 22 August 2022; Accepted: 7 January 2023;
Published online: 18 January 2023

REFERENCES

1. Gupta, A., Sakthivel, T. & Seal, S. Recent development in 2D materials beyond graphene. *Prog. Mater. Sci.* **73**, 44–126 (2015).
2. Akinwande, D. et al. A review on mechanics and mechanical properties of 2D materials—graphene and beyond. *Extreme Mech. Lett.* **13**, 42–77 (2017).
3. Khan, K. et al. Recent developments in emerging two-dimensional materials and their applications. *J. Mater. Chem. C* **8**, 387–440 (2020).
4. Dagdeviren, O. E., Acikgoz, O., Grütter, P. & Baykara, M. Z. Direct imaging, three-dimensional interaction spectroscopy, and friction anisotropy of atomic-scale ripples on MoS_2. *NPJ 2D Mater. Appl.* **4**, 1–6 (2020).

5. Cong, X., Liu, X.-L., Lin, M.-L. & Tan, P.-H. Application of raman spectroscopy to probe fundamental properties of two-dimensional materials. *NPJ 2D Mater. Appl.* **4**, 1–12 (2020).
6. Rajapakse, M. et al. Intercalation as a versatile tool for fabrication, property tuning, and phase transitions in 2D materials. *NPJ 2D Mater. Appl.* **5**, 1–21 (2021).
7. Spear, J. C., Ewers, B. W. & Batteas, J. D. 2D-nanomaterials for controlling friction and wear at interfaces. *Nano Today* **10**, 301–314 (2015).
8. Vazirisereshk, M. R., Martini, A., Strubbe, D. A. & Baykara, M. Z. Solid lubrication with MoS_2: a review. *Lubricants* **7**, 57 (2019).
9. Berman, D., Erdemir, A. & Sumant, A. V. Graphene: a new emerging lubricant. *Mater. Today* **17**, 31–42 (2014).
10. Baykara, M. Z., Vazirisereshk, M. R. & Martini, A. Emerging superlubricity: a review of the state of the art and perspectives on future research. *Appl. Phys. Rev.* **5**, 041102 (2018).
11. Zhang, S., Ma, T., Erdemir, A. & Li, Q. Tribology of two-dimensional materials: from mechanisms to modulating strategies. *Mater. Today* **26**, 67–86 (2019).
12. Wyatt, B. C., Rosenkranz, A. & Anasori, B. 2D MXenes: tunable mechanical and tribological properties. *Adv. Mater.* **33**, 2007973 (2021).
13. Rosenkranz, A. et al. Multi-layer $Ti_3C_2T_x$-nanoparticles (MXenes) as solid lubricants–role of surface terminations and intercalated water. *Appl. Surf. Sci.* **494**, 13–21 (2019).
14. Rodriguez, A. et al. The potential of $Ti_3C_2T_x$ nano-sheets (MXenes) for nanoscale solid lubrication revealed by friction force microscopy. *Appl. Surf. Sci.* **535**, 147664 (2021).
15. VahidMohammadi, A., Rosen, J. & Gogotsi, Y. The world of two-dimensional carbides and nitrides (MXenes). *Science* **372**, eabf1581 (2021).
16. Miao, X., Li, Z., Liu, S., Wang, J. & Yang, S. MXenes in tribology: current status and perspectives. *Adv. Powder Mater.* **2**, 100092 (2022).
17. Grützmacher, P. G. et al. Superior wear-resistance of $Ti_3C_2T_x$ multilayer coatings. *ACS Nano* **15**, 8216–8224 (2021).
18. Bao, Z. et al. Role of MXene surface terminations in electrochemical energy storage: a review. *Chin. Chem. Lett.* **32**, 2648–2658 (2021).
19. Serles, P. et al. Friction of $Ti_3C_2T_x$ MXenes. *Nano Lett.* **22**, 3356–3363 (2022).
20. Hu, T. et al. Interlayer coupling in two-dimensional titanium carbide MXenes. *Phys. Chem. Chem. Phys.* **18**, 20256–20260 (2016).
21. Borysiuk, V. N., Mochalin, V. N. & Gogotsi, Y. Molecular dynamic study of the mechanical properties of two-dimensional titanium carbides Ti(n+1)C(n) (MXenes). *Nanotechnology* **26**, 265705 (2015).
22. Borysiuk, V. & Mochalin, V. N. Thermal stability of two-dimensional titanium carbides $Ti_n + 1C_n$ (MXenes) from classical molecular dynamics simulations. *MRS Commun.* **9**, 203–208 (2019).
23. Osti, N. C. et al. Effect of metal ion intercalation on the structure of mxene and water dynamics on its internal surfaces. *ACS Appl. Mater. Interfaces* **8**, 8859–8863 (2016).
24. Zhang, D. et al. Computational study of low interlayer friction in $Ti_{n+1}C_n$ ($n = 1$, 2, and 3) MXene. *ACS Appl. Mater. Interfaces* **9**, 34467–34479 (2017).
25. Deng, Y., Chen, Y., Liu, H. & Yan, X. The effects of the temperature and termination (-O) on the friction and adhesion properties of mxenes using molecular dynamics simulation. *Nanomaterials* **12**, 798 (2022).
26. Martins, L. G. P. et al. Raman evidence for pressure-induced formation of diamondene. *Nat. Commun.* **8**, 1–9 (2017).
27. Meng, Y. et al. The formation of sp3 bonding in compressed BN. *Nat. Mater.* **3**, 111–114 (2004).
28. Shen, P. et al. Linear tunability of the band gap and two-dimensional (2D) to three-dimensional (3D) isostructural transition in WSe_2 under high pressure. *J. Phys. Chem. C* **121**, 26019–26026 (2017).
29. Hu, T. et al. Vibrational properties of Ti_3C_2 and $Ti_3C_2T_2$ (T = O, F, OH) monosheets by first-principles calculations: a comparative study. *Phys. Chem. Chem. Phys.* **17**, 9997–10003 (2015).
30. Zhang, H., Fu, Z., Legut, D., Germann, T. C. & Zhang, R. Stacking stability and sliding mechanism in weakly bonded 2D transition metal carbides by van der Waals force. *RSC Adv.* **7**, 55912–55919 (2017).
31. Guo, Y., Guo, W. & Chen, C. Modifying atomic-scale friction between two graphene sheets: a molecular-force-field study. *Phys. Rev. B* **76**, 155429 (2007).
32. Eder, S. J., Vernes, A. & Betz, G. On the derjaguin offset in boundary-lubricated nanotribological systems. *Langmuir* **29**, 13760–13772 (2013).
33. Lai, T., Chen, R. & Huang, P. Temperature dependence of microscale adhesion force between solid surfaces using an AFM. *J. Adhes. Sci. Technol.* **29**, 133–148 (2015).
34. Li, D., Müller, M. B., Gilje, S., Kaner, R. B. & Wallace, G. G. Processable aqueous dispersions of graphene nanosheets. *Nat. Nanotechnol.* **3**, 101–105 (2008).
35. Li, W.-K., Zhou, G.-D. & Mak, T. in *Structural Chemistry of Hydrogen* Ch. 11 (OUP, 2008).
36. Schall, J. D., Milne, Z. B., Carpick, R. W. & Harrison, J. A. Molecular dynamics examination of sliding history-dependent adhesion in Si–Si nanocontacts: connecting friction, wear, bond formation, and interfacial adhesion. *Tribol. Lett.* **69**, 1–19 (2021).
37. Bernal, R. A. et al. Influence of chemical bonding on the variability of diamond-like carbon nanoscale adhesion. *Carbon* **128**, 267–276 (2018).
38. Cafolla, C. & Voïtchovsky, K. Lubricating properties of single metal ions at interfaces. *Nanoscale* **10**, 11831–11840 (2018).
39. Marian, M. et al. Effective usage of 2d MXene nanosheets as solid lubricant - influence of contact pressure and relative humidity. *Appl. Surf. Sci.* **531**, 147311 (2020).
40. Ghidiu, M., Kota, S., Drozd, V. & Barsoum, M. W. Pressure-induced shear and interlayer expansion in Ti_3C_2 MXene in the presence of water. *Sci. Adv.* **4**, eaao6850 (2018).
41. BIOVIA. BIOVIA Materials Studio. http://www.3ds.com/products-services/biovia/products/molecular-modeling-simulation/biovia-materials-studio (2020).
42. Jain, A. et al. The materials project: a materials genome approach to accelerating materials innovation. *APL Mater.* **1**, 011002 (2013).
43. Martini, A., Eder, S. J. & Dörr, N. Tribochemistry: a review of reactive molecular dynamics simulations. *Lubricants* **8**, 44 (2020).
44. Huygh, S., Bogaerts, A., Van Duin, A. C. & Neyts, E. C. Development of a ReaxFF reactive force field for intrinsic point defects in titanium dioxide. *Comput. Mater. Sci.* **95**, 579–591 (2014).
45. Kim, S.-Y. et al. Development of a ReaxFF reactive force field for titanium dioxide/water systems. *Langmuir* **29**, 7838–7846 (2013).
46. Kim, S.-Y. & van Duin, A. C. Simulation of titanium metal/titanium dioxide etching with chlorine and hydrogen chloride gases using the ReaxFF reactive force field. *J. Phys. Chem. A* **117**, 5655–5663 (2013).
47. Huang, L., Gubbins, K. E., Li, L. & Lu, X. Water on titanium dioxide surface: a revisiting by reactive molecular dynamics simulations. *Langmuir* **30**, 14832–14840 (2014).
48. Curnan, M. T. & Kitchin, J. R. Investigating the energetic ordering of stable and metastable TiO_2 polymorphs using DFT+ U and hybrid functionals. *J. Phys. Chem. C* **119**, 21060–21071 (2015).
49. Selli, D., Motta, S. & Di Valentin, C. Impact of surface curvature, grafting density and solvent type on the PEGylation of titanium dioxide nanoparticles. *J. Colloid Interface Sci.* **555**, 519–531 (2019).
50. Plimpton, S. Fast parallel algorithms for short-range molecular dynamics. *J. Comput. Phys.* **117**, 1–19 (1995).
51. Stukowski, A. Visualization and analysis of atomistic simulation data with OVITO–the Open Visualization Tool. *Model. Simul. Mat. Sci. Eng.* **18**, 015012 (2009).
52. Hoover, W. G. Canonical dynamics: equilibrium phase-space distributions. *Phys. Rev. A* **31**, 1695 (1985).
53. Seredych, M. et al. High-temperature behavior and surface chemistry of carbide MXenes studied by thermal analysis. *Chem. Mater.* **31**, 3324–3332 (2019).

ACKNOWLEDGEMENTS

This work was partly funded by the Austrian COMET-Program (Project K2 InTribology1, No. 872176) and carried out at the "Excellence Centre of Tribology". The computational results presented here were obtained using the Vienna Scientific Cluster (VSC). The authors acknowledge TU Wien Bibliothek for financial support through its Open Access Funding Program. We would like to thank Hansjörg Grützmacher from ETH Zürich for the fruitful discussions on the interlayer bonding during MXene failure.

AUTHOR CONTRIBUTIONS

Q.Y.: acquisition, analysis, and interpretation of data, design and performance of simulations, original draft; S.J.E.: acquisition, analysis, and interpretation of data, original draft, revision; A.M.: interpretation of data, original draft, revision, supervision; P.G.G.: conception and design, interpretation of data, original draft, supervision.

COMPETING INTERESTS

The authors declare no competing interests.

ADDITIONAL INFORMATION

Supplementary information The online version contains supplementary material available at https://doi.org/10.1038/s41529-023-00326-9.

Correspondence and requests for materials should be addressed to Stefan J. Eder.

Reprints and permission information is available at http://www.nature.com/reprints

Publisher's note Springer Nature remains neutral with regard to jurisdictional claims in published maps and institutional affiliations.